Delft University of Technology

Flexible High-Sensitivity Strain Sensor Fabricated with Pdms Micro-Channel Array Using Laser Transmission Pyrolysis Technology

Wang, Shaogang ; Zong, Qihang; Yang, Huiru; Huang, Qianming ; Ye, Huaiyu; French, Paddy

Citation (APA)
Wang, S., Zong, Q., Yang, H., Huang, Q., Ye, H., & French, P. (2024). Flexible High-Sensitivity Strain Sensor Fabricated with Pdms Micro-Channel Array Using Laser Transmission Pyrolysis Technology. In *Proceedings of the 2024 IEEE 37th International Conference on Micro Electro Mechanical Systems (MEMS)* (pp. 367-370). IEEE. https://doi.org/10.1109/MEMS58180.2024.10439302

Important note
To cite this publication, please use the final published version (if applicable).
Please check the document version above.

FLEXIBLE HIGH-SENSITIVITY STRAIN SENSOR FABRICATED WITH PDMS MICRO-CHANNEL ARRAY USING LASER TRANSMISSION PYROLYSIS TECHNOLOGY

Shaogang Wang[1], Qihang Zong[2], Huiru Yang[2], Qianming Huang[2], Huaiyu Ye[2], and Paddy French[1]*
[1]The Faculty of EEMCS, Delft University of Technology, NETHERLANDS and
[2]The School of Microelectronic, Southern University of Science and Technology, CHINA

ABSTRACT

In recent years, flexible strain sensors based on metal cracks have garnered significant interest for their exceptional sensitivity. However, striking a balance between sensitivity and detection range remains a significant challenge, which often limits its wider application. Herein, we introduce an innovative laser transmission pyrolysis technology to fabricate high-performance flexible strain sensors based on (Au) metal cracks with a microchannel array on the PDMS surface. The fabricated flexible strain sensors exhibit high sensitivity, wide detection range, precise strain resolution, fast response and recovery times, and robust durability. Furthermore, this technology has potential applications in microfluidics, microelectromechanical systems, and optical sensing.

KEYWORDS

Stretchable strain sensor, Metal film, UV laser, Laser transmission pyrolysis, PDMS pattering.

INTRODUCTION

The rapid progress in flexible electronics has spurred innovation in health monitoring, human-machine interaction, and electronic skin [1]. Among them, flexible strain sensors play an important role due to their high sensitivity, wide detection range, and high reliability. These sensors are typically divided into four main categories: resistive, capacitive, piezoelectric, and triboelectric [2]. Resistive strain sensors have attracted considerable attention due to their excellent performance, simple fabrication, and low cost [3]. These sensors typically combine conductive materials (such as metallic nanoparticles or low-dimensional substances) with an elastic substrate (such as silicone resin or rubber base) to achieve conductivity and reliability.

Strain sensors achieve high sensitivity due to significant structural changes during strain, leading to drastic changes in conductivity. For instance, crack-based strain sensors attain heightened sensitivity through the processes of crack formation and expansion, coupled with their disconnection and reconnection properties. As reported, Kang et al. developed a crack-based resistive sensor, ingeniously constructed with platinum (Pt) and polyurethane acrylate (PUA), which exhibited exceptional sensitivity (gauge factor of 2000) within a strain range of 0-2% [4]. This study proved that the introduction of cracks into metal film-based strain sensors is an effective strategy to improve their performance.

However, the inherent trade-off between sensitivity and detection range means that an increase in sensitivity will limit the detection range, and it hinders the widespread use of flexible strain sensors in practical applications. Consequently, alongside new material developments, numerous studies have concentrated on advancing the sensing capabilities of devices by refining crack configurations, including adjustments to crack density, spacing, depth, and interconnectivity [5].

Herein, we designed and fabricated a flexible strain sensor based on (Au) metal cracks with microchannel arrays to overcome this limitation. To realize these microchannel arrays quickly and efficiently, we have developed a promising novel technology for patterning the polydimethylsiloxane (PDMS) substrate: the laser transmission pyrolysis (LTP) technology. Unlike the template-based PDMS patterning process using conventional lithography, this method allows direct patterning of PDMS substrates by a computer-controlled laser scanning path. It not only enables the design and fabrication of high-performance flexible strain sensors but also can also provide design guidelines for applications such as microfluidics, microelectromechanical systems, and optical sensing.

METHODS AND MATERIALS

A. Design and Fabrication

Fig. 1 illustrates the six-step design and fabrication process of flexible strain sensors with PDMS-based microchannel arrays where initially, a PDMS (10:1) mixture was prepared, degassed, and cured in a mold at 80℃; next, the PDMS film (50 mm × 42 mm × 1 mm) was coated with a solution containing 10 wt% PVP and ethanol, followed by UV laser patterning to form microchannels; after cleaning to eliminate any residuals, a gold film was strategically deposited on the PDMS using a polyimide photomask; finally, the PDMS film with microchannel arrays and a gold coating was segmented and packaged using liquid metal and shrinkable tubes.
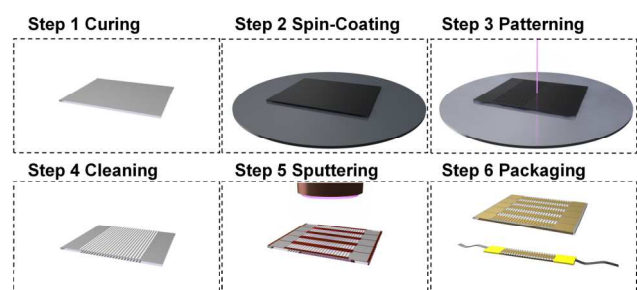

Figure 1: Schematic illustration of the fabrication process for the flexible strain sensor based on Au micro-cracks with a microchannel array.

B. Materials and Equipment

All chemicals were obtained commercially. PDMS

(Sylgard 184) was sourced from Dow Corning. The chosen film ink was Epson BK-T8231. Polyvinyl pyrrolidone (PVP, $(C_6H_9NO)n$, $Mw = 220000$) and anhydrous ethanol (CH_3CH_2OH, 99.5%) were procured from Shanghai Macklin Biochemical Co., Ltd. The liquid metal (metal basis: 99.99% Ga-In-Sn) and single-sided conductive tape (3M7766-50) used in the packaging process were procured from Alfa Aesar Chemical Co., Ltd. and 3M Company, respectively.

The PDMS with microchannel arrays was fabricated using an ultraviolet (UV) pulsed laser system (Grace X 355-3A, Han's Laser Technology Industry Group Co., Ltd., with a wavelength of 355 nm). For laser transmission pyrolysis, the laser was set to a 200 kHz repetition frequency and 1.8 W power. Laser single pulse energy (E_{sp}) was calculated as $E_{sp} = P_{avg}/f_{pr}$. The sputtering power was set at 55 W, the chamber filled with argon (Ar) gas, and the vacuum level maintained at 4 Pa. Commercial single-sided conductive tapes served as connecting wires in the sensor packaging. Liquid metal was applied to these tapes to ensure sensor reliability. Two heat-shrink tubes were then heated at 130 °C for 20 seconds to protect and secure both ends of the sensor.

RESULT AND DISCUSSION

A. Laser Transmission Pyrolysis Technology

Laser transmission pyrolysis ensures the continuity of the photothermal effect by introducing a semi-transparent light-absorbing layer. Specifically, as shown in Fig. 2(a), when the laser is vertically irradiated onto the light-absorbing layer that covers the PDMS surface, most of the laser energy passes through the light-absorbing layer and the PDMS substrate. Only a small portion of the energy is absorbed, which leads to the formation of a laser heating region (LHR). Owing to the photothermal effect, the absorbed energy creates an ultra-high temperature gradient, subsequently triggering the laser pyrolysis reaction within the PDMS. Simultaneously, this process leads to the formation of a hemispherical pyrolysis product within the PDMS, which facilitates heat transfer and forms a heat conduction region (HCR). Finally, the LTP reaction occurs iteratively as the laser moves. Fig. 2(b) shows the SEM image of the PDMS surface following the LTP reaction. The morphology of the sample distinctly delineates both the laser heating and heat conduction regions. Within the laser heating region, the porous pyrolysis products (3C-SiC) are clearly observed.

To realize the regulation of laser transmission pyrolysis, different light-absorbing layers are applied in the laser pyrolysis process. Correspondingly, Fig. 2(c) shows the ultraviolet-visible (UV-Vis) light absorption spectra of PVP in absolute ethanol solutions of film inks with different mass percentages (5, 10, and 15 wt%; labeled as S-5%, S-10%, and S-15%). It is obvious that at a wavelength of 355 nm, the absorption percentages for samples S-5%, S-10%, and S-15% are 10.56%, 17.47%, and 25.21%, respectively, indicating distinct differences. Fig.2 (d) shows that the ability of the light-absorbing layer to absorb UV laser light increases as the mass percentage (wt%) of the film ink increases, leading to an increase in the depth and width of the microchannels. This confirms that adjusting the light-absorbing layer can effectively regulate the reaction intensity of LTP. Notably, within the -0.5 mm and 0.5 mm range around the focal plane, the microchannels created by the LTP reaction on the PDMS surface are of poor quality. In contrast, the best microchannel quality is achieved at defocus distances further from the focal plane (d_{def} = -1 mm and 1 mm).
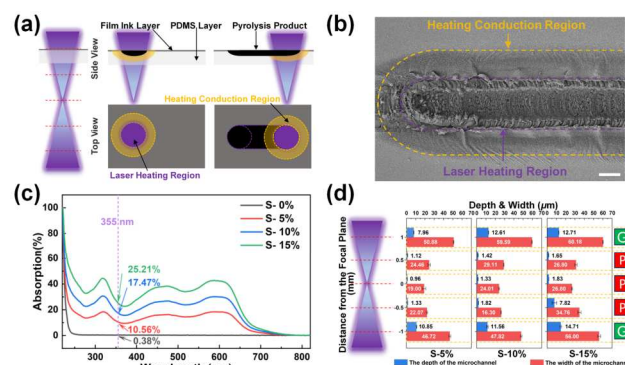

Figure 2: (a) Schematic diagram of the reaction mechanism of laser transmission pyrolysis (LTP). (b) SEM image of PDMS surface after LTP reaction (scale bar: 20 μm). (c) Ultraviolet-visible (UV-Vis) absorption spectra of PVP absolute ethanol solutions with film inks of different mass percentages (0%, 5%, 10%, and 15%). (d) The depth, width, and quality of the microchannel under different light-absorbing layers (wt%) and defocus distances (d_{def}).

B. Performance Test of the Strain Sensor

The fabrication parameters selected for the flexible strain sensor in terms of the UV laser were as follows: an average laser power (P_{avg}) of 1.2 W, a laser repetition frequency (f_{pr}) of 100 kHz, and a laser defocus distance (d_{def}) of 1.0 mm. Using these parameters, we designed and fabricated flexible strain sensors with varying LTP scanning intervals in the microchannel array. We also investigated the effect of metal film thickness on the microchannel array by varying the sputtering times. Fig. 3 (a) illustrates the surface topography of the samples with LTP scanning intervals of 1000 μm, 600 μm, and 200 μm (*I*-1000, *I*-600, *I*-200). Simultaneously, a flat-surface PDMS substrate (*I*-Flat) is used as a control to confirm the performance improvement of the flexible strain sensor. From left to right, the magnetron sputtering deposition times for the samples are set as 10 s, 20 s, and 30 s (labeled as T-10, T-20, and T-30).

Fig. 3(b) shows the relative resistance changes ($\Delta R/R_0$) of flexible strain sensors with both microchannel arrays and flat-surfaces under various strains (ε) during stretching. The addition of microchannels significantly increases the sensitivity of the flexible strain sensor compared to that with the flat-surfaced sensor. For instance, the *I*-Flat&*T*-10 sensor on a flat-surface PDMS substrate reached a GF value of 103.9 after 10 seconds of metal sputtering, calculated within a 40-100% strain range. Remarkably, with a microchannel array (60 μm width, 200 μm interval), the GF value of the *I*-200&*T*-10 sensor soared to 1718.5, representing nearly a 16-fold increase in performance. Consequently, due to the trade-off relationship between sensitivity and detection range, the inherent detection range of the strain sensor with the microchannel array decreased to 69%. Furthermore, the performance of flexible strain

sensors that rely on metal cracks is largely affected by the thickness of the metal film [6]. Clearly, increasing metal sputtering time from 10 to 20 and then to 30 seconds, resulted in the GF values of flat-surface sensors climbing from 103.9 to 183.2 and ultimately to 297.0. Meanwhile, sensors with microchannels experienced a rise in GF values from 1718.0 to 2205.5 and then to 2448.0, coupled with a decrease in detection range from 59% to 45% and finally to 34%.
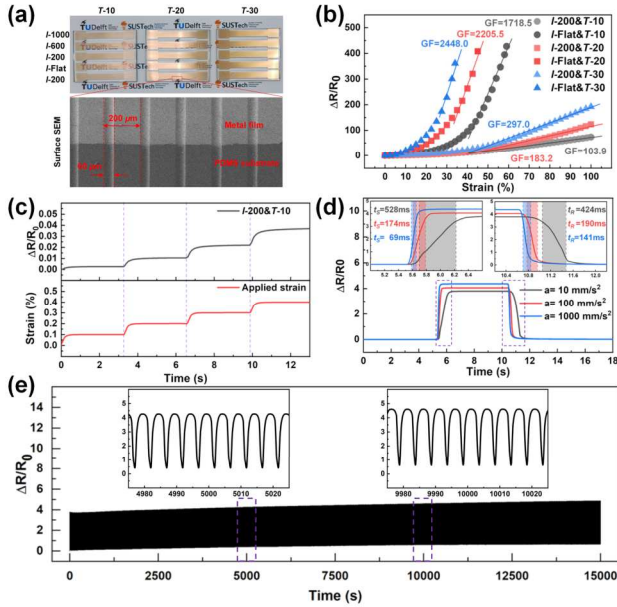

Figure 3: (a) Optical images of different scanning intervals and Au sputtering times, and the SEM image of local microchannel array. (b) Relative resistance changes of strain sensors based on different microchannel arrays and flat-surface under different strains. (c) Relative resistance response curve of the sensor under minor conditions (0.1%). (d) The response time and recovery time of the sensor under different stretch and release accelerations. (e) Relative resistance response curve of the sensor for 3000 stretch-release cycles at 10% strain.

Impressively, the sensor exhibits exceptional strain resolution. As shown in Fig. 3(c), when the sensor is subjected to four consecutive small strains of 0.1%, the change in sensor resistance has a consistent trend with the applied strain. As shown in Fig. 3(d), with increased stretch and release acceleration, both the response and recovery times decrease significantly. It should be noted that, due to the inherent viscoelasticity of PDMS materials, the recovery time consistently exceeds the response time at all levels of tension and release [7]. At maximum acceleration, the response time was measured at 69 ms and the recovery time at 141 ms, respectively. These times align with the operational demands of flexible strain sensors in diverse applications [1]. To assess the long-term reliability of the flexible strain sensor, we applied a constant 10% strain over 3000 cycles at a frequency of 0.2 Hz. Fig. 3(e) reveals that, although minor degradation occurs during stretch-release cycles, the sensor maintains outstanding durability without notable failure.

C. Mechanism Analysis of the Strain Sensor

To investigate the sensing mechanism, we comparatively analyzed the distribution of gold (Au) cracks in flat-surface and microchannel-array sensors under different strain conditions. Fig. 4(a) shows the optical microscopy (OM) images of *I*-Flat&*T*-10 and *I*-200&*T*-10 under tensile strain conditions of 10%, 30%, and 50%. The Au film of the sensor experienced elongation and random cracking perpendicular to the tensile direction when subjected to external strain. This crack propagation trend is consistent with previously reported studies on strain sensors based on metallic cracks [8, 9]. Specifically, the *I*-Flat&*T*-10 sensor exhibited notably lower crack density at 10% strain. In the flat region (R-1) of the PDMS substrate, surface stress induced fractures in the adhering Au film, resulting in crack formation and the release of stretching energy [2]. When the strain was increased to 30%, the number of cracks in the Au film rose noticeably, leading to a significant increase in micro-crack density.

At 50% strain, the micro-crack density in the Au film reached saturation, with further expansion of the micro-crack spacing. In comparison, the Au film of the *I*-200&*T*-10 sensor shows different crack propagation models in the channel and mesa regions (R-2 and R-3) of the PDMS substrate. At 10% strain, the Au cracks in the mesa region (R-3) were basically consistent with the flat region of *I*-Flat&*T*-10. However, the channel region (R-2) exhibited a lower crack density and wider crack spacing. Similarly, as the strain increased to 30%, the crack density in the mesa region increased further. Notably, the crack density in the channel region remained largely stable, but the crack spacing expanded further. At 50% strain, the crack densities in both the mesa and channel regions stabilized, but the crack spacing in the channel region notably widened as external stretching continued. This expansion was the principal cause of the marked change in the relative resistance of the strain sensors with microchannels.
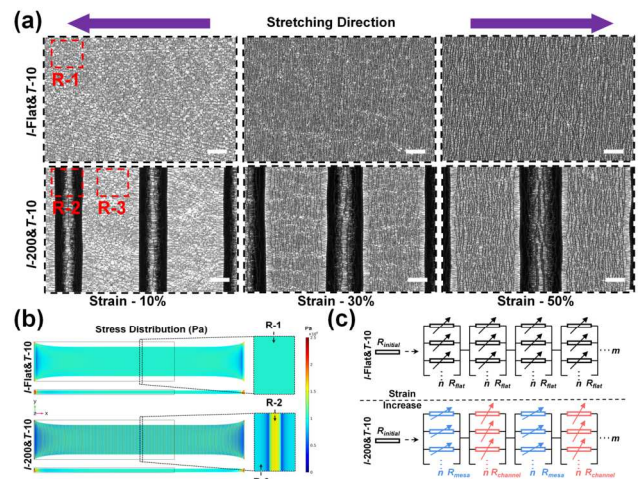

Figure 4: (a) Optical microscope (OM) images of surface Au microcracks distribution of I-Flat&T-10 and I-200&T-10 under 10%, 30%, and 50% tensile strain conditions (scale bar: 50 μm). (b) Strain distribution of PDMS substrates with smooth surface and microchannel array under 50% strain state. (c) Equivalent circuit diagrams corresponding to PDMS substrates with the flat surface and the microchannel array.

369

To investigate the influence of microchannel arrays on crack formation mechanisms in flexible sensors, we employed finite element method (FEM) to simulate deformation and strain distribution within the PDMS substrate. As shown in Fig. 4(b), when subjected to a large strain of 50%, the channel region (R-2) of the PDMS substrate with the microchannel arrays exhibits significantly higher stress compared to the adjacent mesa region (R-3). This indicates that the stress redistribution strategy for PDMS surfaces can be effectively realized by introducing microchannel arrays.

The total resistance of the sensor with a flat surface (R_{FS}) is modeled as a network of resistors composed of m columns, each consisting of n resistors in parallel, expressed as:

$$R_{FS} = \frac{m}{n} R_{flat} \tag{1}$$

where the R_{falt} is the resistance across the crack gap in the flat surface sensor. Correspondingly, the total resistance of the sensor with a microchannel array (R_{MA}) takes into account the differing resistances in the channel and mesa regions, defined as:

$$R_{MA} = \frac{m}{2n} (R_{channel} + R_{mesa}) \tag{2}$$

where the $R_{channel}$ and R_{mesa} are the resistance of the crack gaps in the channel and mesa regions, respectively.

The equivalent circuit diagrams in Fig. 4(c) illustrate that for flat-surface sensors, initial strain primarily induces crack formation, increasing both m and n in the network, with m increasing faster due to cracks aligning perpendicular to strain. As the strain increases, the crack expands further, leading to saturation of m and n. However, the crack gap resistance (R_{flat}) increases significantly, thus dominating the resistance change. For microchannel-array sensors, the channels redistribute the stress distribution on the PDMS, causing different crack propagation models. Compared to the mesa regions, the tensile stress is significantly more concentrated in the microchannel regions. As strain increases, the change in channel resistance ($R_{channel}$) is much greater than that in mesa resistance (R_{mesa}). Despite lower saturation crack density compared to flat-surface sensors, the increased crack spacing in microchannel sensors significantly enhances sensitivity due to greater resistance changes.

CONCLUSION

In summary, we have successfully developed a flexible strain sensor based on gold (Au) cracks, featuring a microchannel array fabricated using laser transmission pyrolysis technology. Through extensive experimentation, we have revealed its operating conditions and the mechanism of pyrolysis. Utilizing this technology, we implemented a surface stress redistribution strategy for microchannel arrays on PDMS surfaces, which resulted in a dramatic increase in the sensitivity of the sensors with microchannel arrays compared to conventional flat-surface sensors. The sensor exhibited high sensitivity (GF of 2448), excellent strain resolution (0.1%), wide detection range (59%), fast response and recovery times (69 ms and 141 ms, respectively), and robust durability (over 3000 cycles). The sensor exhibited high sensitivity (GF = 2448), excellent strain resolution (0.1%), wide detection range (59%), fast response and recovery times (69 ms and 141

ms, respectively), and robust durability (over 3000 cycles). This study offers a promising technology solution for the design and fabrication of high-performance flexible strain sensors based on metal cracks, opening up vast possibilities for their application in health monitoring, human-machine interaction, and electronic skin.

REFERENCES

[1] J. Jung, K. K. Kim, Y. D. Suh et al., "Recent progress in controlled nano/micro cracking as an alternative nano-patterning method for functional applications," Nanoscale Horizons, vol. 5, no. 7, pp. 1036-1049, 2020.

[2] M. Amjadi, K. U. Kyung, I. Park et al., "Stretchable, skin-mountable, and wearable strain sensors and their potential applications: a review," Advanced Functional Materials, vol. 26, no. 11, pp. 1678-1698, 2016.

[3] C. Zhang, J. Sun, Y. Lu et al., "Nanocrack-based strain sensors," Journal of Materials Chemistry C, vol. 9, no. 3, pp. 754-772, 2021.

[4] D. Kang, P. V. Pikhitsa, Y. W. Choi et al., "Ultrasensitive mechanical crack-based sensor inspired by the spider sensory system," Nature, vol. 516, no. 7530, pp. 222-226, 2014.

[5] M. Amjadi, M. Turan, C. P. Clementson et al., "Parallel microcracks-based ultrasensitive and highly stretchable strain sensors," ACS applied materials & interfaces, vol. 8, no. 8, pp. 5618-5626, 2016.

[6] R. Zhou, Y. Zhang, F. Xu et al., "Hierarchical Synergistic Structure for High Resolution Strain Sensor with Wide Working Range," Small, pp. 2301544, 2023.

[7] E. K. Dimitriadis, F. Horkay, J. Maresca et al., "Determination of elastic moduli of thin layers of soft material using the atomic force microscope," Biophysical journal, vol. 82, no. 5, pp. 2798-2810, 2002.

[8] D. Kang, P. V. Pikhitsa, Y. W. Choi et al., "Ultrasensitive mechanical crack-based sensor inspired by the spider sensory system," Nature, vol. 516, no. 7530, pp. 222-226,a2, 2014.

[9] B. Park, J. Kim, D. Kang et al., "Dramatically enhanced mechanosensitivity and signal-to-noise ratio of nanoscale crack-based sensors: effect of crack depth," Advanced materials, vol. 28, no. 37, pp. 8130-8137, 2016.

CONTACT

*Paddy French; p.j.french@tudelft.nl